

Synchronous clusters in a noisy inhibitory neural network

P.H.E. Tiesinga^{1,2*} and Jorge V. José¹

¹ Center for Interdisciplinary Research on Complex Systems,
and Department of Physics, Northeastern University, Boston MA 02115, USA.

² Sloan Center for Theoretical Neurobiology, Salk Institute,
10010 N. Torrey Pines Rd., La Jolla, CA 92037.

arXiv:cond-mat/9904085v1 [cond-mat.stat-mech] 7 Apr 1999

*Corresponding author, Tel: 619 453 4100 ext 1039, Fax: 619 455 7933, E-mail: tiesinga@salk.edu

Keywords: inhibition, neural network, synchronization, noise, information

We study the stability and information encoding capacity of synchronized states in a neuronal network model that represents part of thalamic circuitry. Our model neurons have a Hodgkin-Huxley-type low threshold Calcium channel, display post inhibitory rebound, and are connected via GABAergic inhibitory synapses.

We find that there is a threshold in synaptic strength, τ_c , below which there are no stable spiking network states. Above threshold the stable spiking state is a cluster state, where different groups of neurons fire consecutively, and each neuron fires with the same cluster each time. Weak noise destabilizes this state, but stronger noise drives the system into a different, self-organized, stochastically synchronized state. Neuronal firing is still organized in clusters, but individual neurons can hop from cluster to cluster. Noise can actually induce and sustain such a state below the threshold of synaptic strength. We do find a qualitative difference in the firing patterns between small (~ 10 neurons) and large (~ 1000 neurons) networks.

We determine the information content of the spike trains in terms of two separate contributions: the spike time jitter around cluster firing times, and the hopping from cluster to cluster. We quantify the information loss due to temporally correlated interspike intervals. Recent experiments on the locust olfactory system and striatal neurons suggest that the nervous system may actually use these two channels to encode separate and unique information.

I. INTRODUCTION

The brain receives an enormous amount of information transduced by peripheral sense organs. This massive information influx is coded and decoded in ways that are not yet fully understood in cognitive neuroscience. Recent studies have focussed on specific neural substrates for binding mechanisms. Binding is the process by which the brain combines different aspects of sensory modalities of one object into one unified percept. The neural mechanisms that underlie synchronization in different parts of the brain are only partly understood. There is the suggestion that synchronization may be relevant to binding [1]. Recent experiments have shown that inhibitory interneurons in the hippocampus [2], the thalamic reticular nucleus [3], and the locust olfactory system [4] can indeed synchronize neuronal discharges. Subsequent theoretical analysis of networks of interneurons has shown that strong synchronization by mutual inhibition is only moderately robust against neuronal heterogeneities [5] and synaptic noise [6]. In strong synchronization all the neurons fire with a short time-interval from each other.

In most experiments to date one measures the activity of one neuron, or a small population of neurons. Periodic oscillations (extracellular, or subthreshold intracellular) measured in these experiments are consistent with strong as well as weak synchronization. In weak synchronization the *average* neuronal activity is periodic, without each individual neuron having to fire at each period. Often theoretical analyses, however, have focussed on strong synchronization. Here we conjecture that weak synchronization is robust against neuronal heterogeneities and synaptic noise, and consequently it is much more likely to occur in neuronal systems. Furthermore we show that it can encode more information compared to strongly synchronized states. We present numerical results of weak synchronization in a simple model of a network of Thalamic neurons that supports our conjecture. We use a thalamic network, as an example, due to the wealth of modeling information that is already available. The mechanism we discuss here, however, has more general applicability.

The thalamus acts as a relay for most of the sensory information that travels to cortical structures. It regulates sleep-wake cycles [3] and it may be involved in early stimulus binding [7]. The lateral geniculate nucleus (LGN) and thalamic reticular nucleus (TRN) that are involved in vision have been studied extensively. Neurons of the thalamus express low threshold Calcium currents [8], and they rebound after a sustained hyperpolarization. It has been shown experimentally and in model calculations that inhibitory neurons can synchronize neuronal discharges in the thalamus [9–13] and produce traveling waves [14–17].

The hallmark of weak synchronization is multimodal interspike interval (ISI) histograms (ISIH). The ISI occurs only near multiples of a particular time-scale, e.g. the period of the population activity T . Multimodality of the ISIH has been observed in the LGN [18], and it was attributed to the action of inhibitory neurons. Multimodal ISIH have also been found in model simulations of coupled inhibitory networks in

the presence of noise [19] and in systems exhibiting stochastic resonance (SR) due to a periodic drive [20]. A theoretical mechanism for autonomous stochastic resonance (ASR) was proposed in a recent paper [21]. There the periodic drive was replaced by a periodic mode in an internal kinetic variable, such that the spikes ride on top of subthreshold voltage oscillations. In our work the periodic neuronal activity in the noise-driven system is self-induced by the network. This mechanism is absent in unconnected single neurons, or in a single element with aut synaptic feedback.

It has been suggested that the brain may encode information through an ensemble or cluster of neurons that fire within a short time of each other [22,23]. A particular neuron may be part of a cluster for a few cycles, before it joins another neuronal ensemble. This type of dynamics is very similar to the neuronal clusters that form in our model simulations described below. An important problem is how to quantify the information content of these binding-like cluster states. The Shannon entropy has been used as a measure of information content in investigations of sensory neurons in, for instance, crickets [24], and flies [25]. It is, nonetheless, not known how the brain processes information, and thus it is not clear whether the Shannon entropy is the correct quantity for this purpose. It does, however, provide an upper bound on the theoretical information content of spiking neurons. It also implies that noise in the nervous system contains information, and that noisy neurons are transmitting more information compared to regular noiseless spiking neurons. We emphasize that this statement is still controversial [26–28], because even if the entropy measure yields consistent results in sensory systems this does not guarantee its relevance to the central nervous system. With these caveats in mind we still proceed to characterize the information content of our neural networks by calculating its well-defined Shannon entropy.

One would like to calculate both the output entropy of the model system and the mutual information. The mutual information quantifies how the ensemble of outputs is related to one of the possible realizations of the input, and it involves additional averagings over a conditional probability distribution which makes it very hard to calculate. Even the simpler calculation of the Shannon entropy from its definition in terms of the spike times is a difficult calculation. Here we shall focus on the Shannon entropy of the neuronal output of a neuron as part of the complete network. We also present here some approximations that allows us to estimate the Shannon entropy using the interspike interval time series.

II. METHODS

A. Network model

Our single neuron model equation contains a low threshold Calcium current I_{Ca} , a general leak current I_L , a synaptic current I_{syn} , and a noise current $C_m\xi$,

$$C_m \frac{dV}{dt} = -I_{Ca} - I_L - I_{syn} - C_m\xi, \quad (1)$$

together with the first order (Hodgkin-Huxley type) kinetic equations for the activation m and inactivation h variables for I_{Ca} and the synaptic variable s . This yields a neuronal dynamics in terms of four variables, V , m , h , and s . We have used the kinetics for I_{Ca} and I_{syn} as specified in [14] (a detailed description of the model is given in Appendix A). Our single neuron model captures some important features of the dynamics of thalamic neurons, in particular its post inhibitory rebound (PIR). We are presently studying a more complete model, incorporating thalamo-cortical relay neurons and GABAergic thalamic reticular neurons [15], including all the relevant active currents [29,30]. Our preliminary results suggest that this does not change the conclusions of our discussion here.

The neurons in our network are connected all-to-all by inhibitory GABAergic synapses. Previous studies [16,17] have shown that the precise spatial connectivity is important for the activity propagation. In this work, we will not consider the spatial characteristics of the neuronal activity. We have studied different sized systems, varying from $N = 1$ (a single neuron with aut synaptic feedback) to $N = 1000$. We also have included two types of noises in our model, either Gaussian current noise, characterized by $\langle \xi \rangle = 0$ and

$$\langle \xi(t)\xi(0) \rangle = 2D\delta(t), \quad (2)$$

with D the strength of the noise, or with Poisson distributed excitatory post-synaptic potentials (EPSPs) and inhibitory post-synaptic potentials (IPSPs). In our previous work we have shown that these two types of noises are not fully equivalent [31]. Both can generate, however, similar statistics, and theoretically Gaussian noise is easier to control and vary. The results presented here are thus obtained with Gaussian noise. Unless stated differently the physiological total synaptic conductance used is $g_s = 2 \text{ mS/cm}^2$, and the decay time of the synaptic channel $\tau_s = 16 \text{ ms}$. The noise strength D is expressed in units of mV^2/ms , time in ms, currents in $\mu A/cm^2$, and voltage in mV.

The resulting differential equations for V_i , m_i , h_i , s_i are numerically integrated using a noise-adapted second order Runge-Kutta algorithm [6] with a time-step $dt = 0.1 \text{ ms}$. The calculation starts with random initial conditions, with the initial voltage chosen from a uniform distribution with a range of 20 mV centered around -68 mV , and m , h , and s are set equal to their asymptotic values for a given value of V .

B. Calculated quantities

The raw model output are the time-traces for V_i , m_i , h_i , and s_i . The spike-times are defined as the time when the voltage V_i crosses -30 mV from below. We determined the standard histograms of interspike intervals [32]. The instantaneous firing rate, or frequency f , is defined as the number of action potentials per second in a bin of 2 ms. Both the ISI histogram and f are averaged over all neurons in the network. We also calculated

$$v_{syn} = \frac{1}{N} \sum_i s_i, \quad (3)$$

which is proportional to the current drive due to the synaptic connections with other neurons (and itself). Because the network is connected all-to-all, v_{syn} is the same for each neuron and represents an averaged or mean field type drive. The variable h determines the excitability of the neuron, and the state of the network strongly depends on the h -value distribution. When v_{syn} is below a certain value the network is disinhibited and will fire shortly. To determine the h -distribution prior to firing we have chosen $v_{syn} = 0.01$ as the threshold. This value is reached every cycle, except in the presence of strong noise. In that case the disperse nature of the firing creates an average value of v_{syn} above 0.01. We have determined both the instantaneous as well as the time-averaged distribution of h .

III. RESULTS

The model considered here contains an inward low threshold Calcium current, I_T , that initiates the Calcium action potentials. It is inactivated at the resting membrane potential (RMP, equal to -65.57 mV), and it is de-inactivated at hyperpolarized voltages. For the neuron to be excitable, h has to be de-inactivated (i.e. $h > 0.305$). We illustrate this in Fig.1(a). There are two V null-clines drawn, one (I) in the absence of a current, and the other (II) in the presence of a constant hyperpolarizing current $i = -1 \mu A/cm^2$. We apply a short (10ms) and a long pulse (200ms) with strength i . The phase point moves to II, and the h value starts increasing with time-scale $\tau_1 = 500 \text{ ms}$ (see Appendix A). Upon termination of the short pulse the phase point moves back to I, without generating an action potential (AP). When the long pulse ends, however, the h -value is too high, and the phase point misses the nearby branch of I, and generates an AP.

The necessary hyperpolarization is supplied by the inhibitory postsynaptic potential (IPSP) generated by the activity of other neurons in the network. The strength of the IPSPs is determined by the value of the synaptic conductance g_s and the decay time τ_s . The critical value for periodic oscillations is defined as $\tau_s = \tau_c(g_s, N)$, that depends on the number N of neurons in the network. For $\tau_s < \tau_c$ the oscillation dies out after a finite number of action potentials. In Fig. 1(b) we show the voltage trace oscillations below and above threshold for $N = 1$ (single neuron with aut synaptic feedback). At the start of the simulation the neuron is released from a hyperpolarized voltage. For subthreshold values of τ_s the neuron produces a few spikes before returning to RMP. During each spike the average h value decreases, since the inhibitory drive is not strong enough to replenish the loss due to the depolarization of the AP. Above threshold a periodic spike train is produced. The h -value varies periodically, it decreases during the AP and it increases during the inhibition. Note that the interspike intervals are determined by τ_s . The subthreshold spike train has therefore a much smaller ISI compared

to the one above threshold. We have determined the boundary between stable and unstable oscillations as function of g_s (Fig. 1(a)). The minimum duration τ_s of the IPSP needed for deinactivation, increases for weaker synaptic coupling g_s . The situation for a real network ($N > 1$) is more complicated, since the initial voltages play an important role. If, for instance, we would start with neurons clamped at their resting membrane potential nothing will happen. To obtain a spiking network state we therefore always start the simulations with part or all the neurons clamped at hyperpolarizing voltages. With uniform initial conditions all neurons are clamped at the same voltage value. The threshold τ_c for self-sustained oscillations is then equal to the one for a single neuron (Fig.2(a)). Above threshold this network is in a coherent state: all neurons spike at the same time. For random initial conditions the initial voltage is chosen from a uniform distribution with a range of 20 mV around a hyperpolarized average value. In that case the network can sustain stable oscillations for lower values of τ_s (Fig.2(b)). The network settles in a state where groups of neurons fire simultaneously. It is easy to understand why such cluster states emerge. Starting from random initial conditions each neuron will have a different phase, and will thus reach the AP threshold at a different time. The first neurons to fire will cause an inhibition that blocks other neurons (further from threshold) from firing. They can only fire after the decay of the inhibition (a few τ_s). Periodic oscillations in the network are sustained by inhibition waves produced by the activity of de-inactivated neurons. The oscillations automatically become coherent, with the initial phase differences between cluster neurons driven to zero. In the simplest cluster state each neuron fires with the same ISI. The time between consecutive cluster firings, or cycle length, may vary since the strength of inhibition depends on the cluster size. Neurons will only fire when v_{syn} is below a certain value: the higher the initial value (proportional to cluster size), the longer it takes to reach this value. More complex cluster states may also contain neurons that fire with different frequencies.

Sufficiently strong noise can induce and maintain a spiking network state even for $\tau_s < \tau_c$. Again we have to distinguish between single neurons and a network. The noise-induced dynamics of a single neuron with aut synaptic feedback will not yield a periodic spike-trace. Instead, the ISI distribution has a peak for short times due to ISIs within the spike trains, and an exponential distribution for the intervals between the end of one, and the start of another spike train. We show some representative voltage traces in Fig. 3(c). Close to threshold and with weak noise the neuron produces a long transient that dies out eventually. Stronger noise can spontaneously induce a spike. The inhibition induced by the AP then manages to produce a short spike train. The number of spikes in this train depends on the distance from threshold. This makes the dynamics discussed here essentially different from Stochastic Resonance, since in that case one would obtain a multimodal distribution, with peaks at multiples of the driving frequency.

We studied the dynamics of the cluster states in a network with $N = 1000$, in terms of the variables shown in Figs. 4 and 5. We focused on four values for $D = 0, 0.0024, 0.008, \text{ and } 0.8$. An important variable in our analysis is h , the inactiva-

tion variable of I_T , since the model neuron is only excitable when h is large enough. The distribution of h values in the network will tell us which neurons are excitable, and which ones need to be de-inactivated by further inhibition cycles. The regularity of the network dynamics is further reflected in the periodicity of f and v_{syn} (Fig. 5) and their autocorrelation function (not shown). Note that v_{syn} itself acts as a drive on the neurons. The larger the distance between the peak and trough, the stronger the synchronizing force.

We can identify four different types of regimes. For zero noise ($D=0$) the system is in a state with five clusters of unequal size. The distribution of cluster sizes is determined by the initial conditions. At each time a neuron can only have one of five h -values. This set of h -values goes through a modulation with a period of five cycles (Fig 4(a)). The derived quantities V , h , v_{syn} , and f (Fig. 5(a)) go through the same modulations. When all the clusters have the same size, there are no such modulations, and the h histogram would consist of only 5 peaks.

Immediately after firing, the neuron is partially de-inactivated with each subsequent cycle until it is excitable again (see the h time traces in Fig. 5). The neuron then has to wait its turn to become disinhibited and fire before other clusters do. When there is noise, there is dispersion in the spike firing times. In the absence of time delay there is only a short time interval during which neurons can fire before the inhibition blocks all other firings during one cycle. As a result, clusters lose neurons whose AP has been noise delayed, and other clusters gain those neurons as members. In addition, noise can cause neurons to fire before the rest in their cluster.

Weak noise ($D=0.0024$) disorders the system. The network starts out with unequal cluster sizes (due to the initial conditions). Large clusters lose more neuron members than smaller ones. Weak noise, however, is not strong enough to equalize their numbers on the time-scale considered (5×10^4 ms). Instead the cluster sizes start to vary in a somewhat stochastic fashion, leading to an erratic firing rate (Fig. 4(b)) and a fluctuating period. The time-averaged h histogram is very broad (Fig. 5(b)).

For stronger noise ($D=0.008$) the average cluster size becomes stationary after a brief transient. The h -values that the neurons of different clusters cycle go through are, on the average, the same. As a result there are six smooth peaks in the h -histogram. The peaks become sharper for more de-inactivated values, and the h -distribution is stationary (on the average it is the same for each cycle). The actual neurons that fire in each cluster changes with time. This state is stable up to a noise strength of approximately $D=1$ (for $N=1000$).

The cycle-to-cycle fluctuations in cluster sizes increases with increasing D . The inhibition that each cluster receives (proportional to v_{syn}) varies, and as a result the width of the peaks in the h histogram increases. The cluster size also decreases with increasing D , and the amplitude of v_{syn} oscillations also decreases. The stability of a cluster can be defined as the fraction of neurons that are still part of a given cluster the next time it fires. This is related to the number and height of the peaks in the ISIH (see Fig. 7(a) and (b)), and it decreases with D . The neuron spends most of its time in an

excited state (flat part of $h(t)$, Fig. 5(d)) waiting for its noise induced AP threshold to fall in the inhibition free window. For that reason it is unlikely to fire with the same cluster as in the previous time. Finally, for larger noise strengths, $D > 1$, the firing is no longer organized in clusters, since the noise has become so large that during an inhibition free window not enough neurons fire coherently to create a large enough inhibition to block the discharge until the next cycle. As a result there are no quiescent periods defining cycles and no distinct cycles either.

The cluster states can be quantitatively described by the average cycle length (period), and the periodicity (number of cycles) of the response. We have studied these two quantities as a function of D for different values of τ_s for $N=1000$, and for different system sizes for $\tau_s = 16$. For smaller τ_s the amount of inhibition available for de-inactivation is lower, and the periodicity increases since the de-inactivation has to be spread out over more cycles. The cycle-period, being proportional to τ_s , also decreases. In addition, the oscillation needs a higher minimum value of D to sustain itself, since the average cluster size is given by the system size over the periodicity. When it becomes too small, the periodic component in the inhibition becomes too small, and as a result the cluster state dies. The noise strength for which this happens is only weakly dependent on τ_s . Note that the periodic component is proportional to the cluster size normalized by the network size, in addition it decreases with increasing jitter. There is, however, a difference between large networks ($N \sim 1000$) and small ones ($N \sim 10$). For small networks, a single neuron can provide enough inhibition to block neuronal discharge and thus to maintain a periodic network state. The state is very robust against noise, even when noise reduces the cluster to its minimum size (one neuron), it can still maintain a spiking state. The drawback is that the fluctuations in cluster size will be of the order of the cluster size itself, causing the cycle length to vary considerably. Below threshold (not shown) the amount of noise needed to induce a spiking state increases, and for very small networks ($N < 4$) failure can occur, i.e. the network becomes quiescent if one neuron fails to fire. Note that the maximum periodicity that the system can sustain is bounded by the system size. In Fig. 6 we see that the periodicity obtained for a given D decreases with N .

We now discuss the possible information content of the ISI time series of individual neurons. We assume that the states are characterized by a periodic population activity. This is reflected in the ISI time series because the ISI will only take values close to multiples of the cycle length. The ISIH will therefore consist of a series of peaks. If a neuron would consistently spike with the same cluster, there would be only one peak. The peak with maximum weight is close to the average ISI (and periodicity) of the network, the other peaks correspond to the ISI where the neuron changed cluster. The relative weight of the maximum peak is thus a measure of the stability of the clusters. In Figs. 7(a), and 7(b) we show the ISIH of a state with stable and unstable clusters, respectively. The width of each peak represents the jitter around a multiple of T . We find that the ISIH of an individual network neuron is to a very good approximation the same as the population

averaged ISIH. This does not mean that all the neurons fire independently, it only states that all individual neurons have identical properties, and that in the long run the statistics of their time-series are the same. Our analysis is therefore performed on the population averaged ISIH, and we also use the population averaged return map. We find that the ISIH is well described by a sum of Gaussians (SOG) of different widths (see Appendix B), and that the width increases with the peak number. In Appendix B we derive an expression given in Eq. (B6) for the entropy of the SOG. We see that the number of peaks and their weight –cluster hopping– and their width – jitter within the cluster– yield two distinct contributions to the information encoding capacity. In Fig. 7(c) we plot the entropy as a function of width σ (taken constant for all peaks) and the total number of n peaks (weighted with a cosine envelope, Eq. (B11)). In our simulations we find that the amount of jitter and the number of peaks are closely correlated, and grow with D .

Our present entropy calculations assume that there is no correlation between consecutive ISIs. For a given amount of correlation γ (see Appendix B) the entropy per spike will decrease. We have quantified this in a model calculation for $n = 2$ and various amounts of correlation γ (see Fig. 7(d)).

IV. DISCUSSION

In recent years considerable attention, as well as controversy, has been directed at studying the variability of neuronal discharge in the cortex [28]. It is beyond doubt that neurons *in vivo* are noisy. The question is whether exact spike-times matter – that is, if the jitter in spike times represents information, for instance quantified by the Shannon entropy – or if only the average firing rate matters. If spike times *do* matter, then the synchronized discharge has a special significance. An important question is whether the nervous system is sensitive to synchronization or not. Our work is relevant in shedding light to this fundamental question in two ways. We have shown that noisy neurons can synchronize without the need of a strong external drive, and that the synchronized neuronal discharge has a potentially high information content. To place our results in a proper context we will now discuss these points in more detail below.

The role that inhibitory interneurons play in the functioning of the nervous system has long been unclear. It is hard to find, and to record from interneurons, because they are rather small. Moreover the output of the nervous system is mostly generated by the principal neurons, so early investigations studied mainly the pyramidal neurons. In recent years it has become clear that inhibition plays a major role in synchronizing principal neurons, in for example the hippocampus [33], the thalamus [3], and the locust olfactory system [4]. The mechanism by which synchronized oscillations are generated in the brain is only partly understood. *In vivo* many different rhythms of different frequency have been observed. Pharmacological manipulations of slices in *in vitro* experiments have elucidated some aspects of the synchronization mechanism.

For instance, Whittington *et al* [33] showed that GABA_A-mediated inhibition is responsible for the synchronization in hippocampal slices. Slice experiments, however, suffer from the drawback that the natural afferents are cut, and therefore the synaptic activity giving rise to the *in vivo* variability is absent. Recent theoretical work has shown that in fact synchronization by mutual inhibition is not robust against neuronal heterogeneities [5] and synaptic noise [6]. In theoretical investigations one usually only considers strong synchronization. In strong synchronization one imposes the strong constraint that each neuron has to fire within a short interval from each other. Here we propose that weak synchronization may in fact be more prevalent in networks connected by chemical synapses. In weak synchronization the *average* neuronal activity is periodic, without each individual neuron having to fire at each period. Weak synchronization is for example consistent with the experiments in [33]. There are exceptions. For example, recent experiments on weakly electric fish show that neurons in the pacemaker nucleus are strongly synchronized [34]. There, however, synchronization can possibly be attributed to electric gap junctions.

Weak synchronization is associated with a periodic drive. This drive is either generated externally, as is the case with Stochastic Resonance [20,35], or it is generated intrinsically by the network as it happens here. The neuron then skips periods, which it can either do deterministically (usually one peak in ISIH), or stochastically (multimodal ISIH). In both cases the network dynamics consists of clusters of neurons firing together. But in the latter case the neuronal composition of the clusters varies with time. A neuron that at a certain point fired with a certain cluster A, can fire the next time with another cluster B. This mechanism yields a synchronization that is robust against noise, and neuronal heterogeneity.

Oscillating neural assemblies do play an important role in the functioning of the invertebrate nervous system. In a series of seminal experiments on the bee and locust olfactory system, Laurent *et al.* have shown that different odors activate overlapping ensembles of projection neurons [36]. The periodic discharge of the ensembles is coherent on a cycle-by-cycle basis. Odors may be classified from the temporal firing pattern of projection neurons [37]. Synchronization of the projection neurons may be abolished by applying picrotoxin, and without changing their individual response characteristics [4]. This desynchronization was shown to impair the ability of bees to distinguish two closely related odors [22], and subsequently a population of neurons was found that was sensitive to the synchronization of projection neurons [38]. The ability to distinguish between two odors, based on their spike trains, was then reduced under desynchronized conditions.

We find that the information content, defined by the Shannon entropy of the spike-time distribution, contains three contributions. First, the jitter in the spike times around the cluster firing time. Second, the distribution of the number of cycles between two consecutive spikes, and finally the correlation between consecutive ISIs. Our analysis has been performed on the (average) output of a single neuron. One has to await the development of fast computational techniques to tackle the more challenging problem of quantifying the information out-

put of the network, while taking into account the correlation in spike times between different neurons due to the cluster state. Our single-neuron spike-train results, however, may have direct relevance to recent experimental work on striatal neurons [39]. Striatal neurons can be in the down (hyperpolarized, quiescent), or in the up-state (depolarized, noisy). The transitions to the up-state are precisely timed and synchronous. The fine-structure in the spike train is asynchronous. Wilson *et al.* [39] have suggested that the brain may use these two channels to encode different types of information.

We have studied the dependence of these oscillations on network parameters. We find that there is difference between small (around ten neurons) and large networks (a few hundred neurons), under the conditions of having a fixed total synaptic drive per neuron. For small networks one needs more noise to drive the subthreshold network into stable oscillations. These oscillations are very robust against increases in the noise level, and the fluctuations in the time between two cluster firings (cycle length) increases with the amount of noise. For large networks strong noise causes an instability, the stable cluster size for a given amount of noise becomes too small to inhibit out of sync neuronal discharges. For intermediate noise-strengths the neuronal dynamics self-organizes itself into a stochastically synchronized state. We also find that the farther the network is below threshold, more noise is necessary to induce a spiking state. The mechanism to create the oscillations is due to the competition between the excitatory de-inactivating, and the inhibitory effect of the synaptic drive. Each cycle will de-inactivate neurons, until they are excitable again. The neuron then has to await the decay of inhibition created by more excitable neurons. For some parameter values the latter stage is absent, and the dynamics is fully deinactivation dominated. The important time-scales in the dynamics are the deinactivation time-scale τ_1 and the synaptic decay time τ_s . The cycle or population period scales directly with τ_s . Our results therefore predict that by pharmacologically decreasing τ_s one can increase the cycle frequency.

In summary, the brain has circuitry capable synchronizing with heterogeneous components, and in the presence of noise. The spike trains of the synchronized discharge still contain information. Whether the brain utilizes this mechanism to synchronize, and more importantly whether it uses the information in the precise temporal sequence is still an open question awaiting further study.

V. ACKNOWLEDGEMENTS

This work was partially funded by the Northeastern University CIRCS fund, and the Sloan Center for Theoretical Neurobiology (PT). We thank TJ Sejnowski for useful suggestions.

-
- [1] Singer W and Gray CM. Visual feature integration and the temporal correlation hypothesis. *Annu. Rev. Neurosci.*, pages 555–586, 1995.
- [2] Whittington MA, Traub RD, and Jeffreys JGR. Synchronized oscillations in interneuron networks driven by metabotropic glutamate receptor activation. *Nature*, 373:612–615, 1995.
- [3] Steriade M, McCormick DA, and Sejnowski TJ. Thalamocortical oscillations in the sleeping and aroused brain. *Science*, 262:679–685, 1993.
- [4] MacLeod K and Laurent G. Distinct mechanisms for synchronization and temporal patterning of odor-encoding neural assemblies. *Science*, 274:976–979, 1996.
- [5] Wang XJ and Buzsáki G. Gamma oscillation by synaptic inhibition in a hippocampal interneuronal network model. *J. Neurosci.*, 16:6402–6413, 1996.
- [6] Tiesinga PHE, Rappel W-J, and José, JV. Synchronization in networks of noisy interneurons. In Bower J, editor, *Computational Neuroscience*, pages 555–559. Plenum Press, New York, 1998.
- [7] Sillito AM, Jones HE, Gerstein GL, and West DC. Feature-linked synchronization of thalamic relay cell firing by feedback from the visual cortex. *Nature*, 369:479–482, 1994.
- [8] Jahnsen H and Llinás R. Ionic basis for the electroresponsiveness and oscillatory properties of the guinea-pig thalamic neurons in vitro. *J. Physiol.*, 349:227–247, 1984.
- [9] Wang X-J and Rinzel J. Spindle rhythmicity in the reticularis thalami nucleus: synchronization among mutually inhibitory neurons. *Neuroscience*, 53:899–904, 1993.
- [10] Wang X-J, Golomb D, and Rinzel J. Emergent spindle oscillations and intermittent burst firing in a thalamic model: specific neuronal mechanisms. *Proc Natl Acad Sci USA*, 92:5577–5581, 1995.
- [11] Golomb D and Rinzel J. Synchronization properties of spindle oscillations in a thalamic reticular nucleus model. *J. Neurophys.*, 72:1109–1126, 1994.
- [12] von Krosigk M, Bal T, and McCormick DA. Cellular mechanisms of a synchronized oscillation in the thalamus. *Science*, 261:361–364, 1993.
- [13] Bal T, von Krosigk M, and McCormick DA. Synaptic mechanisms underlying synchronized oscillations in the ferret lateral geniculate nucleus in vitro. *J. Physiol.*, 483:641–663, 1995.
- [14] Rinzel J, Terman D, Wang XJ, and Ermentrout B. Propagating Activity Patterns in Large-Scale Inhibitory Neuronal Networks. *Science*, 279:1351–1355, 1998.
- [15] Destexhe A and Sejnowski TJ. Synchronized oscillations in thalamic networks: insights from modeling studies. In Steriade M, Jones EG, and McCormick DA, editors, *Thalamus*. Elsevier, 1996.
- [16] Destexhe A, Bal T, McCormick DA, and Sejnowski TJ. Ionic mechanisms underlying synchronized oscillations and propagating waves in a model of ferret thalamic slices. *J. Neurophys.*, 76:2049–2070, 1996.
- [17] Golomb D, Wang XJ, and Rinzel J. Propagation of spindle waves in a thalamic slice model. *J. Neurophysiol.*, 75:750–769, 1996.
- [18] Funke K, Nelle E, Li B, and Wörgötter F. Corticofugal feedback improves the timing of retino-geniculate signal transmission. *Neuroreport*, 7:2130–2134, 1996.
- [19] Golomb D and Rinzel J. Clustering in globally coupled inhibitory neurons. *Physica D*, 72:259–282, 1994.
- [20] Wiesenfeld K and Moss F. Stochastic resonance and the benefits of noise: from ice ages to crayfish and SQUIDS. *Nature*, 373:33–36, 1995.
- [21] Longtin A. Autonomous stochastic resonance in bursting neurons. *Phys. Rev. E*, 55:868–876, 1997.
- [22] Stopfer M, Bhagavan S, Smith BH, and Laurent G. Impaired odor discrimination on desynchronization of odor-encoding neural assemblies. *Nature*, 390:70–74, 1997.
- [23] Riehle A, Grun S, Diesmann M, and Aertsen A. Spike synchronization and rate modulation differentially involved in motor cortical function. *Science*, 278:1950–1953, 1997.
- [24] Levin JE and Miller JP. Broadband neural encoding in the cricket cercal sensory system enhanced by stochastic resonance. *Nature*, 380:165–168, 1996.
- [25] Rieke F, Warland D, de Ruyter van Steveninck RR, and Bialek W. *Spikes: exploring the neural code*. MIT press, Cambridge, 1997.
- [26] Softky WR and Koch C. The highly irregular firing of cortical cells is inconsistent with temporal integration of random EPSPs. *J. Neurosci.*, 13:334–350, 1993.
- [27] Shadlen MN and Newsome WT. Noise, neural codes, and cortical organization. *Curr. Opin. Neurobiol.*, 4:569–579, 1994.
- [28] Shadlen MN and Newsome WT. The variable discharge of cortical neurons: implications for connectivity, computation, and information coding. *J. Neurosci.*, 18:3870–3896, 1998.
- [29] Huguenard JR and McCormick DA. Simulation of the currents involved in rhythmic oscillations in thalamic relay neurons. *J. Neurophys.*, 68:1373–1383, 1992.
- [30] McCormick DA and Huguenard JR. A model of the electrophysiological properties of thalamocortical relay neurons. *J. Neurophys.*, 68:1384–1400, 1992.
- [31] Tiesinga PHE and José, JV. Spiking Statistics in Noisy Hippocampal Interneurons. *Proceedings Computational Neuroscience 1998*, 1999.
- [32] Rodieck RW, Kiang NY-S, and Gerstein GL. Some quantitative methods for the study of spontaneous activity of single neurons. *Biophys. J.*, 2:351–368, 1962.
- [33] Traub RD, Whittington MA, Colling SB, Buzsáki G, and Jeffreys JGR. Analysis of gamma rhythms in the rat hippocampus in vitro and in vivo. *J Physiol*, 493:471–484, 1996.
- [34] Moortgat KT, Keller CH, Bullock TH, and Sejnowski TJ. Sub-microsecond pacemaker precision is behaviorally modulated: the gymnotiform electromotor pathway. *Proc. Natl. Acad. Sci.*, 95:4684–4689, 1998.
- [35] Gluckman BJ, Netoff TI, Neel EJ, Ditto WL, Spano ML, and Schiff SJ. Stochastic resonance in a neuronal network from a mammalian brain. *Phys. Rev. Lett.*, 77:4098–4101, 1996.
- [36] Laurent G and Davidowitz H. Encoding of Olfactory information with oscillating neural assemblies. *Science*, 265:1872–1875, 1994.
- [37] Wehr M and Laurent G. Odor-encoding by temporal sequences of firing in neural assemblies. *Nature*, 384:162–165, 1996.
- [38] MacLeod K and Laurent G. Who reads temporal information contained across synchronized and oscillatory spike trains. *Nature*, 395:693–698, 1998.

- [39] Stern EA, Jeager D, and Wilson CJ. Membrane potential of simultaneously recorded striatal spiny neurons in vivo. *Nature*, 394:475–478, 1998.

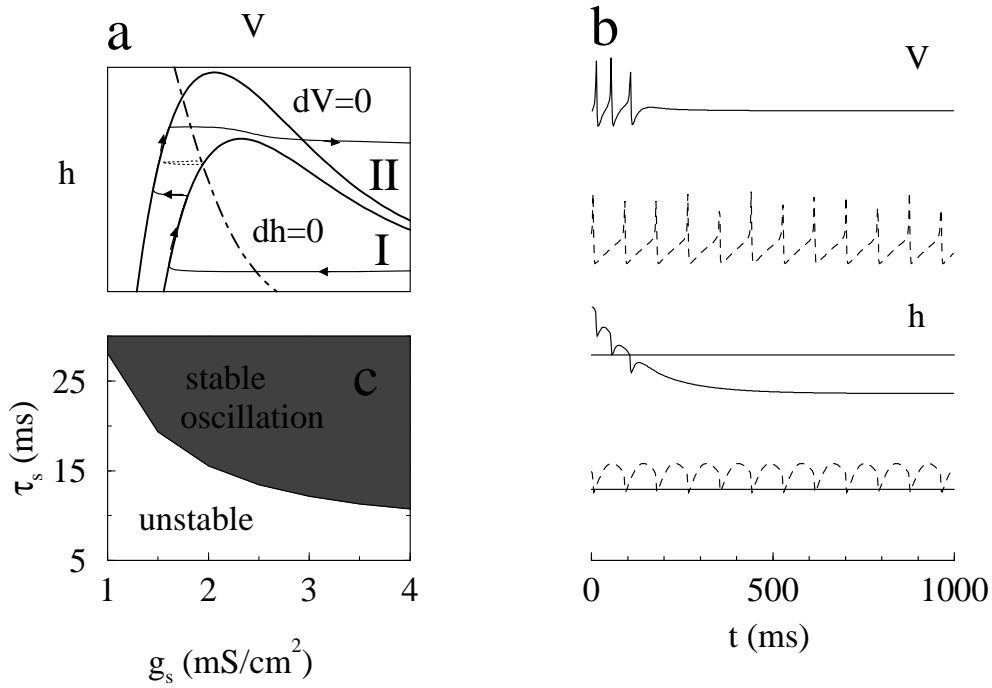


FIG. 1. (a) Phase-plane plots of the neuronal dynamics for the variables h and V . The plotted nullclines correspond to $dh/dt = 0$ (dot-dashed line), and $dV/dt = 0$ (solid lines), $I = -1.0$ (top) and $I = 0.0$ (bottom). The phase trajectory of a neuron released after 10 ms (dotted), and 200 ms (dashed) with hyperpolarizing current pulse $I = -1$. (b) Top curves for V , and bottom curves for h , plotted as a function of time for $\tau_s = 5 \text{ ms} < \tau_c$ (solid lines), and curves $\tau_s = 16 \text{ ms} > \tau_c$ (dashed), with $g_s = 2.0$. (c) Phase-diagram τ_s vs. g_s . Stable oscillations for $\tau_s > \tau_c(g_s)$ are shaded while the unstable ones $\tau_s < \tau_c(g_s)$ are colored white.

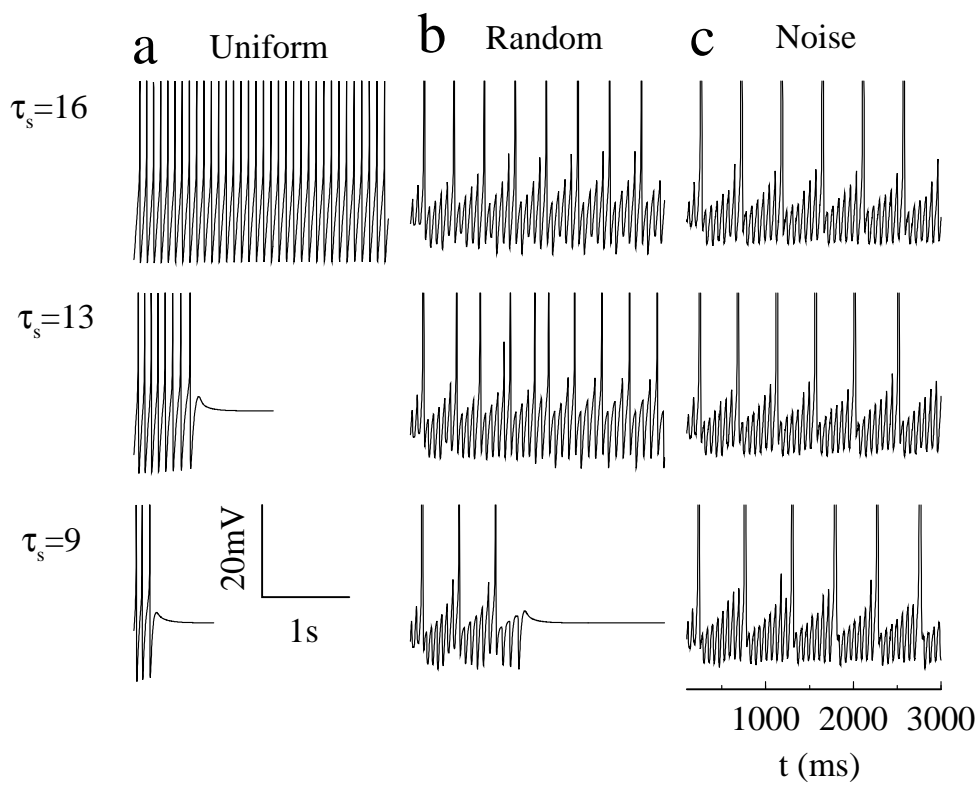


FIG. 2. Voltage traces for neuron one of an $N = 1000$ neuron network of all-to-all connected with (a) uniform initial conditions, (b) random initial conditions, (c) uniform initial conditions with noise ($D = 0.02$, without the transient of 100 ms), for three different values of $\tau_s = 16, 13, 9$ (from top to bottom). A voltage and time scale bar is shown in the lower left graph.

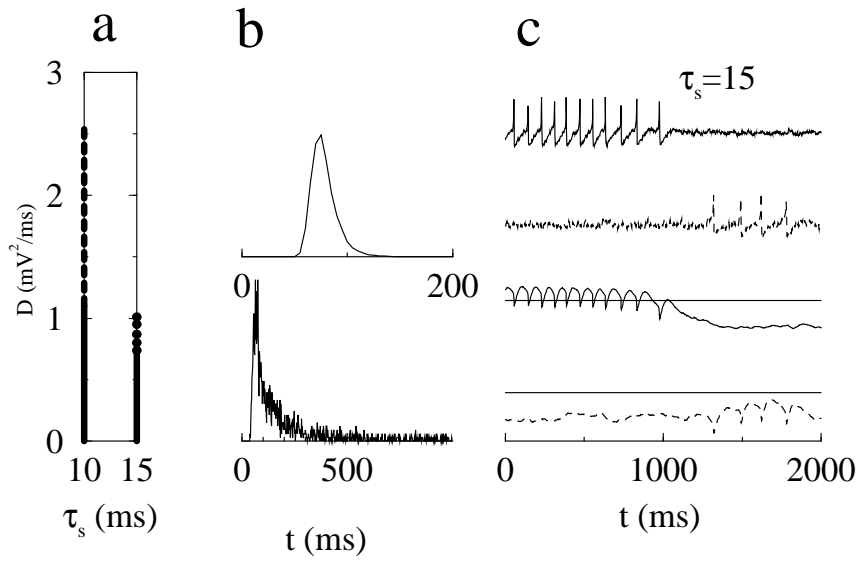


FIG. 3. Noise-driven single neuron dynamics with aut synaptic feedback. (a) Phase-diagram of neuronal behavior as function of noise strength D , for different values of τ_s . No activity (solid line), spontaneous single spikes (dashed line), spontaneous spike-trains (filled circles). (b) ISIH for (top) $\tau_s = 15$ and $D = 0.76$; (bottom) $\tau_s = 10$ and $D = 2$. (c) Representative voltage (top) and h (bottom) time traces for $D = 0.26$ (solid lines) and $D = 0.76$ (dashed lines) with $\tau_s = 15$.

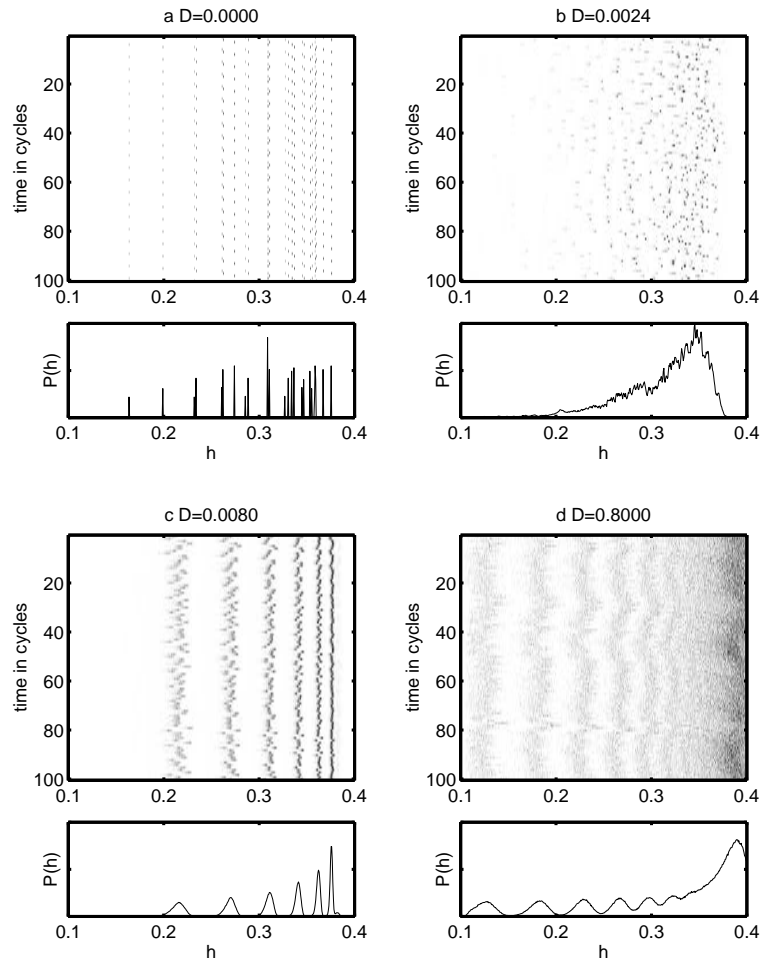


FIG. 4. Each panel consists of a gray-scale coded instantaneous h value distribution for consecutive cycles (top), and the time-averaged h distribution (over at least 500 cycles) (bottom). From left to right, top to bottom the noise-values are $D = 0, 0.024, 0.08, 0.8$. In the upper left panel (a) the delta function peaks in the h -distribution have been broadened to enhance visibility.

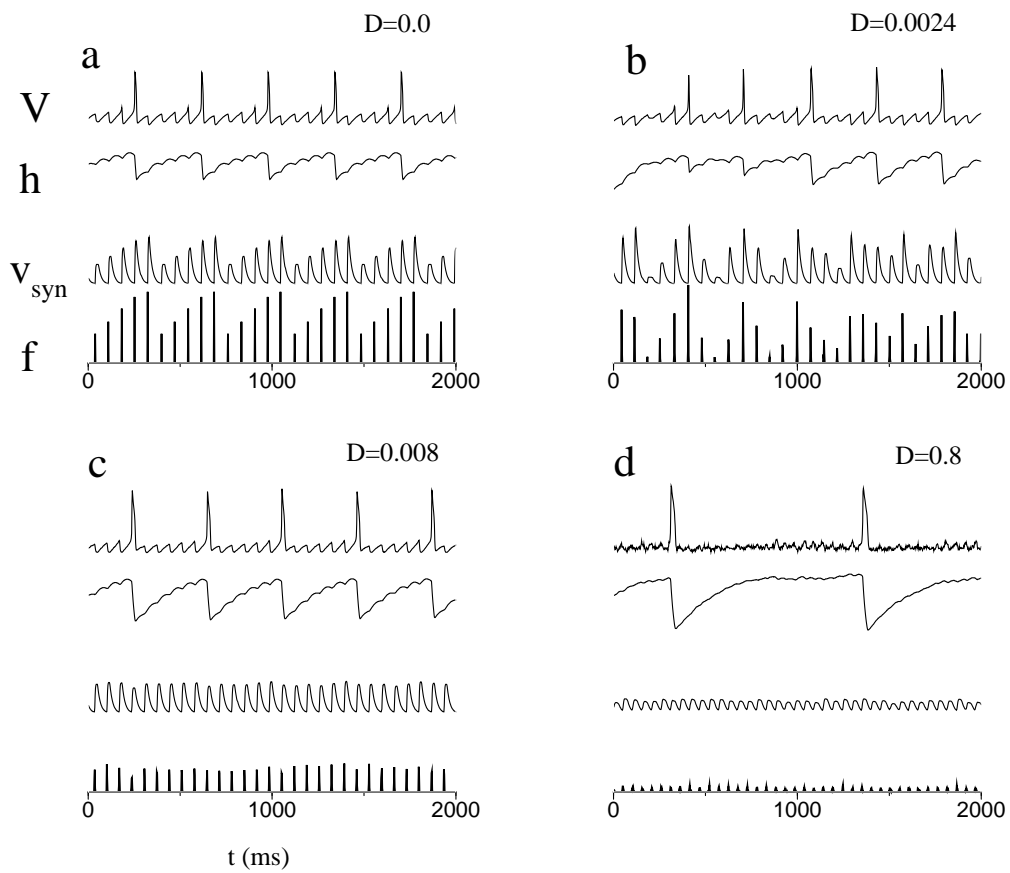


FIG. 5. Four panels with the same D values given in Fig. 4: from left to right, top to bottom the noise-values are $D = 0, 0.024, 0.08, 0.8$. We plot in each panel from top to bottom the V and h functions of neuron one, the population average v_{syn} of the synaptic variables s_i , and the instantaneous firing rate f as a function of time.

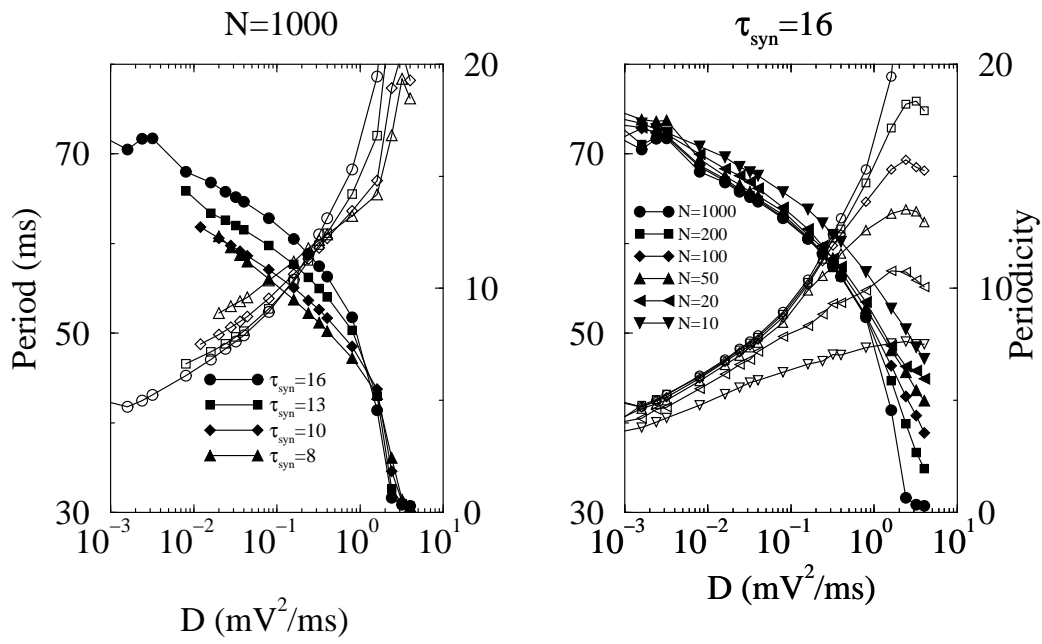


FIG. 6. Here we plot the average period (filled symbols, left hand scale), and the periodicity (open symbols, right hand scale) as a function of D , for $\tau_s = 8, 10, 13, 16$ (for $N = 1000$) and for different system sizes $N = 10, 20, 50, 100, 200$, and 1000 .

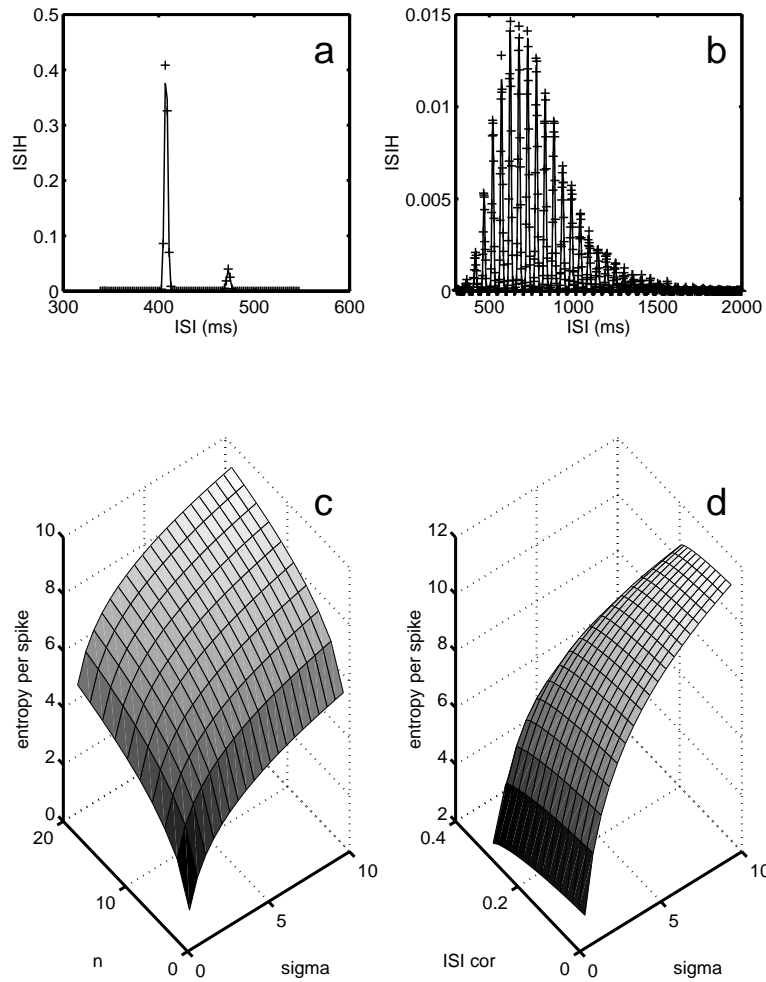


FIG. 7. We plot the ISIH (+) and the corresponding SOG (continuous line) for (a) $D = 0.008$ and (b) $D = 0.8$, both for $N = 1000$, and $\tau_s = 16$. We show the entropy per spike (c) as a function of the number of states n and the jitter σ ; (d) as a function of the amount of correlation between consecutive ISI and σ .

APPENDIX A: MODEL EQUATIONS

In this appendix we more specifically define the models studied in this paper. The dynamics of the voltage V and the kinetic variables h , s , and m are given by the following equations,

$$\begin{aligned} C_m \frac{dV}{dt} &= -I_{Ca} - I_L - I_{syn} - C_m \xi, \\ \frac{dh}{dt} &= (h_\infty - h)/\tau_h, \\ \frac{ds}{dt} &= k_f F(V_{pre})(1 - s) - s/\tau_{syn}, \\ m &= m_\infty(V). \end{aligned}$$

Here the currents are

$$\begin{aligned} I_L &= g_l(V - E_L), \\ I_{Ca} &= g_{Ca} m_\infty(V) h(V - E_{Ca}), \\ I_{syn} &= g_{syn} s_{tot}(V - E_{syn}). \end{aligned}$$

The asymptotic values of the kinetic variables, and the h time-scale, are specified by

$$\begin{aligned} m_\infty &= 1/[1 + \exp -(V + 40)/7.4], \\ h_\infty &= 1/[1 + \exp(V + 70)/4], \\ \tau_h &= \phi(\tau_0 + \tau_1/[1 + \exp(V + 50)/3]). \end{aligned} \tag{A1}$$

The synaptic activity is implemented in a standard way [9]. F is chosen such that a presynaptic depolarization higher than -35 mV will open the synaptic channels.

$$F(V) = 1/[1 + \exp -(V + 35)/2]. \tag{A2}$$

The total synaptic coupling in our all-to-all network is defined as

$$s_{tot} = \frac{1}{N} \sum_i s_i, \tag{A3}$$

and is the same for each neuron.

The standard physiological set of parameters we use in our calculations have the conductances $g_L = 0.4$, $g_{Ca} = 1.5$, and $g_{syn} = 2.0$ (in mS/cm²), the reversal potentials $E_L = -70$, $E_{Ca} = 90$, $E_{syn} = -85$ (in mV), and $C_m = 1\mu F/cm^2$, $\tau_0 = 30$, $\tau_1 = 500$ (in ms), $k_f = 0.5ms^{-1}$, and $\phi = 1.3$.

APPENDIX B: SHANNON ENTROPY CALCULATION

As mentioned in the main body of the paper, we quantify the information content in the ISI using the Shannon entropy,

$$S = - \int \mathcal{D}(\{t_i^n\}) \mathcal{P}(\{t_i^n\}) \log_2 \mathcal{P}(\{t_i^n\}), \tag{B1}$$

for the distribution of the spiking times. In this expression t_i^n is the i th spike time of the n th neuron, and \mathcal{D} is the sum over all spiking time possibilities within a $[0, T]$ interval. We do not try to evaluate this quantity for the whole network, since at present it is a very hard calculation to do. Here we will instead calculate the one neuron entropy in the network, which is expressed in terms of the distribution $P(\{\tau_n\})$ of interspike intervals τ_n , as

$$\begin{aligned} S &= - \int \mathcal{D}(\{\tau_n\}) p(\{\tau_n\}) \log_2 p(\{\tau_n\}) \\ &\approx -\langle N \rangle \int d\tau P_{ISIH}(\tau) \log_2 P_{ISIH}(\tau), \end{aligned} \tag{B2}$$

with $\langle N \rangle$ the average number of events during time interval T . We also assume that consecutive ISIs are randomly independent,

$$p(\tau_1, \dots, \tau_N) = \prod_n P_{ISIH}(\tau_n). \quad (\text{B3})$$

As explained in the main body of the text the ISIH obtained from our simulations is, to a good approximation, a sum of Gaussians (SOG), i.e.,

$$P_{ISIH}(\tau) = \sum_i c_i G(\tau | \mu_i, \sigma_i), \quad (\text{B4})$$

where

$$G(\tau | \mu_i, \sigma_i) = \frac{1}{\sqrt{2\pi\sigma_i^2}} \exp[-(\tau - \mu_i)^2 / 2\sigma_i^2], \quad (\text{B5})$$

with average μ_i , standard deviation σ_i , and c_i is the relative weight for the i -th Gaussian contribution. From the calculated ISIH, we estimate these parameters from the weight c_i , the average μ_i , and the standard deviation σ_i of the i th peak. When $(\mu_{i+1} - \mu_i) \gg \sigma_i$, for all i , Eq. (B2) reduces to

$$\begin{aligned} S &= \langle N \rangle \left(\sum_i c_i \log_2 2\pi e \sigma_i^2 - \sum_i c_i \log_2 c_i \right) \\ &\equiv S_1 + S_2. \end{aligned} \quad (\text{B6})$$

These are the two contributions to the entropy of a multimodal ISIH. A contribution S_1 due to the jitter around the average ISI value of a given state i , and the contribution S_2 due to the discrete probability distribution of the number of cycles between two spikes. Note that S_1 depends on the accuracy with which the ISI can be recorded and detected (taken to be 1 ms here). In the other limit $(\mu_{i+1} - \mu_i) < \sigma_i$, we numerically evaluate the entropy from Eq. (B2) using the measured (binned) ISIH.

In Eq. (B2) we have assumed that consecutive ISIs are independent. If consecutive ISIs are correlated, however, one can use the theory of Markov chains to evaluate the Shannon entropy of the spike trains. The ISIs can belong to n different states, and they have an equilibrium probability $P_{eq} = (c_1, \dots, c_n)$ to be in any particular state. From a given state i the ISI can jump to a new state j with probability T_{ji} , which we can obtain from a return map. In the return map we plot the next ISI versus the current ISI, and then divide it into a two-dimensional set of bins b_{ji} . The bins are centered on multiples of the cycle length, and their width is also equal to the cycle length, then

$$T_{ji} = b_{ji} / \sum_i b_{ji}, \quad (\text{B7})$$

and when the ISIs are independent, $T_{ji} = c_j$ (i.e. the next state does not depend on the previous state). The actual ISI in each state also displays some jitter, and it is distributed according to some $\phi_i(\tau)$. We will assume that ϕ_i is Gaussian (as before), and the entropy is then given by:

$$\begin{aligned} S &= -\frac{1}{\log 2} [(m+1)I \cdot (T\alpha) \cdot P_{eq} + \sum_i c_i \log c_i + mI \cdot (T \log T) \cdot P_{eq}] \\ &\equiv S_1 + S_2 + S_3. \end{aligned} \quad (\text{B8})$$

We have used the following definitions: $m+1$ is the number of ISIs, $(T\alpha)_{ij} = T_{ij}\alpha_i$ ($T \log T)_{ij} = T_{ij} \log T_{ij}$ (no summations implied), $\alpha_i = \int d\tau \phi_i(\tau) \log \phi_i(\tau)$, and \cdot denotes matrix multiplication. Here we give the explicit formula's for $n = 2$

$$(T\alpha) \equiv \begin{pmatrix} \alpha_1 p & \alpha_2 (1-q) \\ \alpha_1 (1-p) & \alpha_2 q \end{pmatrix}, \quad (\text{B9})$$

$$(T \log T) \equiv \begin{pmatrix} p \log p & (1-q) \log(1-q) \\ (1-p) \log(1-p) & q \log q \end{pmatrix}. \quad (\text{B10})$$

When the ISIs are independent then $S_3 = 0$, and S_1 and S_2 reduce to their expression given in Eq. (B6).

We have evaluated expression Eq. (B6) (see Fig. 7(c)) using

$$\begin{aligned} c_{L+1 \pm i} &= \frac{1}{2\pi} \left(\frac{2}{n} + \sin \frac{2\pi(\pm i + \frac{1}{2})}{n} - \sin \frac{2\pi(\pm i - \frac{1}{2})}{n} \right), \\ \mu_j &= \mu + (j - L)\Delta\mu, \\ \sigma_j &= \sigma. \end{aligned} \quad (\text{B11})$$

Here $n = 2L + 1$, $i = 1, \dots, L$; $j = 1, \dots, n$; and $\Delta\mu$ is the cycle length.

Correlation in consecutive ISIs can be parameterized using a δ , with $q = 1 + \delta - p$ in Eqs. (B9) and (B10). The explicit result for $m = 100$ is plotted in Fig. 7(d).